HHS Public Access

Author manuscript

Cell Metab. Author manuscript; available in PMC 2016 October 06.

Published in final edited form as:

Cell Metab. 2015 October 6; 22(4): 669–681. doi:10.1016/j.cmet.2015.07.027.

Hepatic Mitochondrial Pyruvate Carrier 1 is Required for Efficient Regulation of Gluconeogenesis and Whole-body Glucose Homeostasis

Lawrence R. Gray[1], **Mst Rasheda Sultana**[1], **Adam J. Rauckhorst**[1], **Lalita Oonthonpan**[1], **Sean C. Tompkins**[1], **Arpit Sharma**[1], **Xiaorong Fu**[7,8], **Ren Miao**[10], **Alvin D. Pewa**[1], **Kathryn S. Brown**[3], **Erin E. Lane**[4,5], **Ashley Dohlman**[1], **Diana Zepeda-Orozco**[3], **Jianxin Xie**[11], **Jared Rutter**[9], **Andrew W. Norris**[1,3,5,6], **James E. Cox**[9,10], **Shawn C. Burgess**[7,8], **Matthew J. Potthoff**[2,5,6], and **Eric B. Taylor**[1,5,6,*]

[1]Department of Biochemistry, University of Iowa Carver College of Medicine, Iowa City, Iowa, 52240, USA

[2]Department of Pharmacology, University of Iowa Carver College of Medicine, Iowa City, Iowa, 52240, USA

[3]Department of Pediatrics, University of Iowa Carver College of Medicine, Iowa City, Iowa, 52240, USA

[4]Department of Internal Medicine, University of Iowa Carver College of Medicine, Iowa City, Iowa, 52240, USA

[5]Fraternal Order of the Eagles Diabetes Research Center, University of Iowa Carver College of Medicine, Iowa City, Iowa, 52240, USA

[6]Abboud Cardiovascular Research Center, University of Iowa Carver College of Medicine, Iowa City, Iowa, 52240, USA

[7]Advanced Imaging Research Center, University of Texas Southwestern Medical Center, Dallas, Texas, 75390, USA

[8]Department of Pharmacology, University of Texas Southwestern Medical Center, Dallas, Texas, 75390, USA

[9]Department of Biochemistry, University of Utah School of Medicine, Salt Lake City, UT 84112, USA

[*]Correspondence: eric-taylor@uiowa.edu (E.B.T).

Author Contributions

LRG, AS, AJR, and EBT wrote the manuscript. LRG, AJR, JR, AN, and EBT edited the manuscript. LRG, MST, LO, AN, JEC, SCB, MP, and EBT designed experiments. LRG, MST, LO, AJR, SCT, AS, XF, RM, ADP, KSB, EEL, AD, DZO, MJP, and EBT performed experiments. JR generated mice essential for this research. JX is an employee of Cell Signaling Technology, Inc. and developed proprietary antibodies essential for this research.

[10]Metabolomics Core Research Facility, University of Utah School of Medicine, Salt Lake City, UT 84112, USA

[11]Cell Signaling Technology, Inc., Danvers, MA 01923, USA

Summary

Gluconeogenesis is critical for maintenance of euglycemia during fasting. Elevated gluconeogenesis during Type 2 Diabetes (T2D) contributes to chronic hyperglycemia. Pyruvate is a major gluconeogenic substrate and requires import into the mitochondrial matrix for channeling into gluconeogenesis. Here, we demonstrate that the Mitochondrial Pyruvate Carrier (MPC) comprising the Mpc1 and Mpc2 proteins is required for efficient regulation of hepatic gluconeogenesis. Liver-specific deletion of *Mpc1* abolished hepatic MPC activity and markedly decreased pyruvate-driven gluconeogenesis and TCA cycle flux. Loss of MPC activity induced adaptive utilization of glutamine and increased urea cycle activity. Diet-induced obesity increased hepatic MPC expression and activity. Constitutive *Mpc1* deletion attenuated the development of hyperglycemia induced by a high-fat diet. Acute, virally-mediated *Mpc1* deletion after diet-induced obesity decreased hyperglycemia and improved glucose tolerance. We conclude that the MPC is required for efficient regulation of gluconeogenesis and that the MPC contributes to the elevated gluconeogenesis and hyperglycemia in T2D.

Graphical Abstract

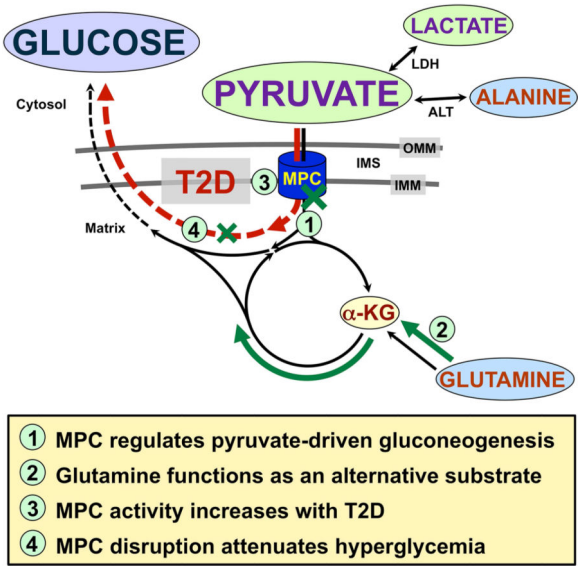

Introduction

Multicellular organisms have evolved complex processes for systemic fuel recycling and maintenance of energy balance. Among the most important of these in mammalian systems is gluconeogenesis, a process whereby products of carbohydrate and amino acid metabolism are condensed and replenished with electrons to form glucose. Gluconeogenesis is critical during prolonged fasting for maintenance of organismal function, especially of the central

nervous system. The liver performs the large majority of whole-body gluconeogenesis with secondary contributions from the kidneys. Despite being essential for survival, excessive gluconeogenesis drives disease, as typified by human patients with Type 2 Diabetes (T2D). In T2D, elevated gluconeogenesis leads to chronic hyperglycemia with devastating consequences, including blindness, kidney failure, and cardiovascular events.

The mechanisms regulating gluconeogenesis are incompletely understood thereby limiting potential treatments for hyperglycemia. The enzyme phosphoenolpyruvate carboxykinase (PEPCK) functions as the key control point of the canonical gluconeogenic pathway by catalyzing the committed step, the conversion of oxaloacetate to phosphoenolpyruvate (Forest et al., 1990). However, upstream factors involving mitochondrial metabolism potently influence gluconeogenesis by regulating provision of oxaloacetate to PEPCK (Burgess et al., 2007).

The vast majority of gluconeogenic carbon flux is routed through the mitochondrial matrix and pyruvate is thought to be the major mitochondrially-imported substrate (Katz and Tayek, 1999; Terrettaz and Jeanrenaud, 1990). Once in mitochondria, pyruvate is channeled towards gluconeogenesis by carboxylation to oxaloacetate by the enzyme pyruvate carboxylase. This reaction regulates oxaloacetate supply to PEPCK and therefore overall gluconeogenic rate. In T2D, elevated hepatic β-oxidation drives gluconeogenesis by raising mitochondrial levels of reducing equivalents and acetyl-CoA, which allosterically activates pyruvate carboxylase (Kumashiro et al., 2013; Merritt et al., 2011). Increased flux through pyruvate carboxylase requires increased mitochondrial pyruvate availability and, therefore, implicates increased activity of the Mitochondrial Pyruvate Carrier (MPC) as a contributor to the excessive gluconeogenesis in T2D.

The MPC conducts pyruvate across the mitochondrial inner membrane to the matrix and thereby occupies a critical link between cytosolic and mitochondrial metabolism. Cytoplasmic pyruvate is derived from multiple sources in the cytosol including glycolysis and systemically-produced lactate and alanine. Pyruvate diffuses freely across the mitochondrial outer membrane through non-selective pores but, like other charged molecules, requires specialized transport across the inner membrane. Therefore, the MPC would be expected to gate pyruvate-driven gluconeogenesis and, in T2D, import pyruvate at the higher rates required for elevated gluconeogenesis.

Initial investigations of the MPC activity in ex vivo liver or kidney systems found that chemical inhibition decreased gluconeogenesis (Halestrap and Denton, 1975; Mendes-Mourão et al., 1975; Thomas and Halestrap, 1981). However, although the MPC has been known as a specific, inhibitable biochemical activity for over 40 years, the proteins of the MPC complex and the genes that encode them remained unidentified until recently.

We and others recently discovered the molecular identity of the MPC (Bricker et al., 2012; Herzig et al., 2012). The mammalian MPC protein complex comprises two obligate, paralogous subunits, designated MPC1and MPC2, which are encoded by the *MPC1* and *MPC2* genes and highly conserved across eukaryotes. MPC1 and MPC2 associate in a heteroligomer of currently unknown but possibly dynamic stoichiometry (Bender et al.,

2015). Loss of either protein results in degradation of the other and loss of MPC activity (Bricker et al., 2012; Herzig et al., 2012; Vigueira et al., 2014).

The identification of the genes encoding the MPC now enables in vivo, molecular-genetic studies on MPC function. We generated mice with liver-specific deletion of *Mpc1* and investigated the importance of the MPC for hepatic gluconeogenesis. We found that the MPC gates pyruvate-driven hepatic gluconeogenesis. We observed that liver-specific disruption of the MPC evokes broad changes in cellular- and systems-level metabolism including adaptive glutaminolysis in the liver and decreased hyperglycemia in mouse models of T2D.

Results

Mpc1 Liver-specific Knockout Mice Display Gross Changes in Metabolism and Maintain Fasting Euglycemia

Mpc1 and Mpc2 proteins are expressed at relatively high levels in the liver, the major site of gluconeogenesis (Figure 1A). To investigate the function of the MPC in vivo for the regulation of hepatic gluconeogenesis, we generated mice with a conditional, floxed *Mpc1* allele ($Mpc1^{fl}$), which was functionally wild-type (Figure S1A, S1B). We successively crossed $Mpc1^{fl/fl}$ (WT) mice with mice expressing Cre under control of the albumin promoter (Alb-Cre) (Postic et al., 1999), resulting in mice with liver-specific *Mpc1* deletion (Mpc1 LivKO) (Figure 1B). Loss of Mpc1 protein was accompanied by loss of Mpc2 protein (Figure 1C), because Mpc1 protein is required for stable expression of Mpc2 protein, and therefore loss of the MPC protein complex. Compared to WT mice, Mpc1 LivKO mice weighed slightly less but displayed no differences in body composition (Figure S1C, S1D), food intake (Figure 1D), and voluntary physical activity (Figure 1E), suggesting the absence of a global energetic defect.

To investigate changes in gross metabolism, we measured gas exchange (Figure 1F) and postabsorptive (4h food restriction) and fasted (18h) serum parameters (Table 1). Mpc1 LivKO mice manifested a decreased respiratory exchange ratio (RER) during the dark cycle when most physically active, increased ketones, decreased cholesterol, decreased fasting triglycerides, and slightly but significantly elevated blood lactate levels, all consistent with decreased gluconeogenesis and increased hepatic and whole-body fat oxidation. Postabsorptive triglycerides were slightly increased. Liver triglycerides and glycogen were not significantly different. Notably, AST/ALT ratios were unchanged, suggesting the absence of liver damage in Mpc1 LivKO mice.

However, although fasting blood glucose levels of Mpc1 LivKO mice tended to be decreased, they were well within normal ranges. Furthermore, glucose and insulin intolerance were not changed (Figure 1G, 1H) and endogenous glucose production was normal during fasting and suppressed normally during euglycemic hyperinsulinemic clamp with no change in peripheral insulin sensitivity (Figure 1I-K, S1E). The absence of an overt defect in glucose homeostasis raised two, non-exclusive possibilities. First, that hepatic pyruvate-driven gluconeogenesis remained intact by an MPC-independent mechanism.

Second, that increased gluconeogenesis through an alternative pathway or site was compensating.

Hepatocyte Mitochondrial Pyruvate Uptake and Pyruvate-driven Respiration are MPC-dependent

To begin to investigate the effects of *Mpc1* deletion on pyruvate-driven gluconeogenesis, we isolated mitochondria from WT and Mpc1 LivKO mouse liver and measured ^{14}C-radiolabeled pyruvate uptake. Importantly, this would test whether the protein complex comprising Mpc1 and Mpc2 functions as the major mitochondrial pyruvate carrier in liver, as we and others had previously shown in yeast, flies, and cultured fibroblasts (Bricker et al., 2012; Herzig et al., 2012). Mpc1 LivKO mitochondria manifested a complete loss of pyruvate uptake (Figure 2A). This result extended to a test of mitochondrial function where pyruvate-driven respiration by Mpc1 LivKO mitochondria was markedly decreased at both higher (Figure 2B) or lower pyruvate concentrations (Figure S2A), which, respectively, increase MPC-dependent or decrease MPC-independent respiration. MPC-independent respiration occurs in vitro because of the super-endogenous pyruvate levels required for adequate signal to noise (Pande and Parvin, 1978). The decrease in pyruvate oxidation by Mpc1 LivKO mitochondria was not amplified by treatment with the MPC inhibitor 4-alpha-hydroxycinnamatic acid (CHC) and matched that for WT mitochondria treated with CHC, both consistent with inhibition of the Mpc1-Mpc2 complex by CHC.

In a parallel experiment, glutamate oxidation, which is also complex I-dependent, was unaffected providing evidence that general mitochondrial respiratory function remained intact despite the absence of the MPC (Figure 2C). Western blots of liver (Figure 2D) or mitochondrial (Figure S2B) lysates for VDAC and mitochondrial respiratory complex proteins showed no changes, indicating that respiratory chain content was unaffected by *Mpc1* deletion. Collectively, these results demonstrated that mitochondrial pyruvate uptake and pyruvate-driven respiration are highly MPC-dependent whereas core respiratory parameters are not.

Pyruvate-driven Hepatic Gluconeogenesis is MPC-dependent

Because of the possibility of an MPC-independent mechanism specialized for gluconeogenic mitochondrial pyruvate uptake, we tested the importance of the MPC for pyruvate-driven glucose production by cultured WT and Mpc1 LivKO mouse primary hepatocytes. Lactate, the reduced form of pyruvate, was co-administered with pyruvate at a ratio of 10:1 to approximate the intracellular ratio and minimize perturbation of redox state. *Mpc1* deletion resulted in a large decrease in glucose production that was not significantly decreased by treatment with the MPC inhibitor UK-5099 (Figure 3A). This result demonstrated that the MPC gates pyruvate-driven gluconeogenesis in cultured hepatocytes.

Because Mpc1 LivKO mice maintained fasting euglycemia, potentially by increased utilization of non-pyruvate substrates, we sought to more specifically test the in vivo importance of the MPC for pyruvate-driven gluconeogenesis. We performed a lactate/pyruvate tolerance test (L/PTT) by intraperitoneal injection of 18 hours-fasted WT and Mpc1 LivKO mice. Blood glucose excursion and lactate clearance were strikingly decreased

in Mpc1 LivKO mice (Figure 3B, 3C), consistent with impaired pyruvate-driven gluconeogenesis. We observed similar results with female mice (Figure S2C, S2D).

We next utilized universally (U) ^{13}C-labeled lactate and pyruvate tracers to measure pyruvate incorporation into glucose. Here, each of the three carbon atoms of lactate or pyruvate is the stable ^{13}C isotope, resulting in a 3 dalton mass increase (M+3). WT and Mpc1 LivKO mice were administered U^{13}C-lactate and -pyruvate by intraperitoneal injection as performed previously (Potthoff et al., 2011). To capture flux data under near-equilibrium gluconeogenic conditions, livers were harvested and immediately freeze-clamped at 30 minutes post-injection, the expected time of plateau for blood glucose and lactate concentrations. The most direct flux of U^{13}C-pyruvate into glucose yields the M+3 glucose isotopomer. Metabolomic analysis of hepatic extracts revealed a markedly lower concentration of M+3 glucose in Mpc1 LivKO mice (Figure 3D). Results were highly similar for the M+2 and total labeled glucose pools, as complementary measures of flux (Table S1). These results provided direct evidence that hepatic pyruvate-driven gluconeogenesis is MPC-dependent. Nonetheless, the important question remained of how Mpc1 LivKO mice maintain fasting euglycemia.

Mpc1 Deletion Results in Impaired Pyruvate-driven TCA Cycle Flux

To identify a potential adaptive pathway by which Mpc1 LivKO mice sustained gluconeogenesis, we extended our flux metabolomics analysis to TCA cycle intermediates. For all intermediates analyzed, which were citrate, α-ketoglutarate (AKG), succinate, fumarate, malate, and oxaloacetate, fractional abundance of the M+3 isotopomer was decreased in Mpc1 LivKO mice, consistent with decreased flux of pyruvate into the TCA cycle (Table S1). However, analysis of absolute M+3 isotopomer concentrations revealed a striking pattern that implicated increased amino acid influx through AKG as a potential adaptation to loss of MPC activity. First, concentrations of M+3 lactate and pyruvate were increased (Figure 4A). Second, M+3 concentrations of citrate, succinate, fumarate, malate, and oxaloacetate were decreased. Third, and in contrast, M+3 concentrations of AKG were not significantly decreased. With closer examination, greater absolute AKG concentrations were off-setting a decreased M+3 fractional enrichment (Table S1), resulting in M+3 AKG concentrations similar to WT. As with glucose, this pattern persisted through the M+2 and total labeled pools (Table S1). These findings suggested that pyruvate and lactate accumulated because of decreased mitochondrial pyruvate uptake, that pools of citrate, succinate, fumarate, malate, and oxaloacetate were strongly MPC-dependent, but that a significant component of the AKG pool was MPC-independent.

We speculated that inflation of the AKG pool in Mpc1 LivKO mice signified increased anaplerotic flux of glutamine into the TCA cycle. We previously showed that fibroblasts isolated from a human patient with an inactivating *MPC1* mutation displayed normal glutamine oxidation (Bricker et al., 2012; Brivet et al., 2003). Here, we observed that Mpc1 LivKO mitochondria oxidized glutamate at normal rates (Figure 2C). Glutaminolysis is a hall-mark of many cancer cells and occurs concomitantly with aerobic glycolysis, which may be promoted by loss of MPC activity (Schell et al., 2014). In cell culture systems, glutamate dehydrogenase-dependent glutaminolysis was increased after disruption of the

MPC (Vacanti et al., 2014; Yang et al., 2014). Therefore, we extended our flux metabolomic analysis to glutamate and glutamine and found that as with AKG, ^{13}C-labeled concentrations were not decreased in Mpc1 LivKO mice, consistent with AKG flux predominating from glutamine rather than pyruvate (Figure 4A, Table S1).

Mpc1 Deletion Decreases Steady-state Fasting Hepatic Glutamine Concentrations Concomitant with Increased Markers of Urea Cycle Activity

To further investigate the adaptive metabolism by which Mpc1 LivKO mice maintain euglycemia during fasting, we performed broad, steady-state metabolomic analysis comparing WT and Mpc1 LivKO mouse livers after 18 hours of fasting. One-hundred and eighteen known metabolites were measured from major hepatic metabolic programs including the TCA cycle, glycolysis, the pentose phosphate pathway, the urea cycle, and general amino acid, lipid, and nucleotide metabolism (Table S2). We expected this experiment would complement our pyruvate-driven flux metabolomics experiments by capturing larger steady-state patterns of compensation. Indeed, principle component analysis (Xia et al., 2012) of aggregate metabolomic data demonstrated that WT and Mpc1 LivKO hepatic metabolisms are systematically distinct (Figure S3A).

Analysis of individual metabolites revealed changes in Mpc1 LivKO livers consistent with decreased pyruvate and increased glutamine flux into the TCA cycle. Lactate and pyruvate were significantly increased (Figure 4B). Glycolytic and pentose phosphate pathway intermediates were unchanged or increased, consistent with increased mass action-driven shunting of glucose into cytosolic metabolism because of impaired downstream flux into mitochondria (Figure S3B). Notably, concentrations of TCA cycle intermediates were generally unchanged, indicating, independent of rates of flux, that pool sizes were maintained (Figure S3B). However, AKG was a distinctive outlier with a marked increase in concentration (Figure 4B). Glutamine and aspartate but not other protein-coding amino acids were significantly decreased (Figure 4B, Figure S3B), consistent with glutamine as a source of AKG. Intriguingly, we observed significant increases in urea, ornithine, and N-acetyl-glutamate (Figure 4B), the obligate activator of the rate-limiting enzyme of the urea cycle, carbamoyl phosphatase. However, this was not surprising because increased urea cycle activity would scavenge the ammonia produced by the increased deamination of glutamine to α-ketoglutarate. Combined with flux metabolomic data where Mpc1 LivKO livers exhibited inflation of an MPC-independent AKG pool with an enrichment pattern similar to glutamate and glutamine, these data suggested that increased glutaminolysis in Mpc1 LivKO mice decreases glutamine concentrations, drives increased AKG concentrations, and generates an ammonia load that activates the urea cycle.

Glutamine Supports Robust MPC-independent Gluconeogenesis

To test the efficacy of glutamine as an MPC-independent gluconeogenic substrate, we measured glutamine-driven gluconeogenesis by WT and Mpc1 LivKO primary hepatocytes. It was not significantly decreased by MPC chemical inhibition or *Mpc1* deletion (Figure 4C). Moreover, glutamine supported a higher rate of glucose production than pyruvate (Figure 3A, Figure 4C). To assess in vivo relevance, we performed an intraperitoneal glutamine tolerance test (QTT) with WT and Mpc1 LivKO mice. In contrast to results

observed with lactate/pyruvate, glutamine-driven glucose excursion in Mpc1 LivKO mice was not impaired (Figure 4D). Interpreted together, these results demonstrated that glutamine robustly supports MPC-independent hepatic gluconeogenesis.

We next investigated potential mechanisms for MPC-independent, pyruvate-driven gluconeogenesis. Though our primary hepatocyte and in vivo flux metabolomic data convincingly demonstrated that loss of MPC activity decreased pyruvate-driven gluconeogenesis, ^{13}C-label from pyruvate continued to be incorporated into glucose, indicating persistence of MPC-independent pyruvate-driven gluconeogenesis. Furthermore, in isolated mouse primary hepatocytes, neither genetic disruption nor chemical inhibition of the MPC eliminated pyruvate-driven gluconeogenesis (Figure 3A). We considered the possibility of cytosolic pyruvate conversions to metabolites that would not require the MPC to enter mitochondria.

Pyruvate is interchangeable to alanine or malate by single reactions, catalyzed by alanine transaminase (ALT) or malic enzyme (ME), respectively, in both the cytosol and mitochondria. Thus, transformation of pyruvate to alanine or malate could enable pyruvate-derived carbon to enter mitochondria independently of the MPC. To examine this possibility, we performed gluconeogenesis assays with isolated primary rat hepatocytes treated with vehicle, the MPC inhibitor UK-5099, the ALT inhibitor β-chloro-alanine (Beuster et al., 2011), or UK-5099 and β-chloro-alanine combined.

Glutamine, alanine, and malate all supported MPC-independent gluconeogenesis, although in varying capacities (Figure 4E). As with mouse primary hepatocytes, lactate/pyruvate-driven gluconeogenesis was markedly decreased by MPC inhibition. ALT inhibition alone exerted a mild but statistically significant effect. Combined MPC and ALT inhibition dramatically decreased gluconeogenesis. In contrast, a combined lactate/pyruvate + glutamine cocktail supported robust gluconeogenesis that was insensitive to MPC, ALT, or combined inhibition. Similar results were obtained with administration of glutamine without lactate/pyruvate. These two results provided evidence for selective utilization of glutamine from media rich in lactate/pyruvate to support MPC-independent gluconeogenesis.

Pyruvate Transformations as a Mechanism for Pyruvate-driven, MPC-independent Gluconeogenesis

Interestingly, a combined lactate/pyruvate and alanine cocktail led to a gluconeogenic rate similar to that for lactate/pyruvate alone, which was not significantly decreased with either MPC or ALT inhibition, but was markedly decreased by combined MPC and ALT inhibition (Figure 4E). A similar pattern was observed for alanine alone but with lesser gluconeogenic rates. Together, these results and those with lactate/pyruvate alone, provide evidence for pyruvate-alanine cycling as an MPC by-pass, where pyruvate may be transaminated to alanine by the cytosolic ALT, imported into mitochondria, and deaminated to pyruvate by the mitochondrial ALT (Figure 4F), as demonstrated in vivo by a co-submitted manuscript (McCommis et. al).

Similar to glutamine, malate alone supported gluconeogenesis that was insensitive to MPC or ALT inhibition but at a lesser rate, closely matching that of alanine (Figure 4E). $NADP^+$-

dependent regulation of cytosolic ME strongly favors malate, thus pyruvate would not be expected to be converted to malate at high rates. Nonetheless, the fraction of lactate/pyruvate-driven gluconeogenesis insensitive to combined MPC and ALT inhibition, although minimal, was greater than that observed for alanine and similar to that for malate alone. This raises the possibility that a minor fraction of MPC-independent, pyruvate-driven gluconeogenesis may be supported by pyruvate-malate interconversions (Figure 4F).

Consideration of Additional Adaptive Responses to Loss of Hepatic MPC Activity

We considered whether changes in hepatic gene expression could contribute to the altered metabolism and serum parameters observed in Mpc1 LivKO mice. We examined transcript abundance by qPCR for components of key metabolic pathways including gluconeogenesis (*Fbp1*, *G6pc*, *Pck1*, *Ppargc1a*, *Pc*), de novo lipogenesis (*Acly*, *Acaca*, *Fasn*, *Srebf1*, *Scd1*), fatty-acid oxidation (*Acox1*, *Cpt1a*, *Echs1*, *Hadha*), and ketogenesis (*Bdh1*, *Bdh2*, *Hmgcs1*), and *Gls2*, the hepatocyte-specific isoform of glutaminase, in ad libitum-fed and 18 hours-fasted WT and Mpc1 LivKO mice (Figure S4). No significant differences were observed between genotypes within the fed or fasted states for enzymes for gluconeogenesis, lipogenesis, and fatty-acid oxidation, or for glutaminase. We note that fasting was accompanied by significant increases in *Fbp1*, *Pck1*, *Ppargc1a*, and *Pc*, consistent with transcriptional upregulation of gluconeogenesis, but an unexpected decrease in *G6pc*. This decrease in *G6pc* was tested and observed again with two additional primer pairs, and again with fresh RNA isolates and cDNA preparations, suggesting that the regulation of *G6pc* is complex and extends beyond feeding status. Under fasting conditions, the abundance of transcripts for ketogenesis or fatty-acid oxidation was decreased or not different in Mpc1 LivKO mice compared to WT mice. This finding is divergent from the increased serum ketones observed in Mpc1 LivKO mice (Table 1), suggesting that fatty acid oxidation and ketogenesis may be increased by regulatory changes in enzyme specific activities or mass action forces resulting from loss of MPC activity.

Finally, because renal gluconeogenesis can compensate for impaired hepatic gluconeogenesis, we measured *Pck1* and *G6pc* transcript abundance in the kidney cortex. Kidney cortex levels of both *Pck1* and *G6pc* increased with fasting. Increases were significantly greater in Mpc1 LivKO compared to WT mice, consistent with potential compensatory upregulation of supplemental renal gluconeogenesis (Figure S4).

Constitutive Loss of Hepatic MPC Activity Attenuates Development of Hyperglycemia and Glucose Intolerance with High Fat Diet-induced Obesity

We reasoned that the MPC might be limiting for the higher rates of gluconeogenesis induced in mice by a high-fat diet, a model for human T2D. WT and Mpc1 LivKO litter-mates were placed on a high-fat diet at age 10 weeks and weight was measured weekly. Postabsorptive blood glucose and insulin were measured every third week. Both groups gained weight at equal rates (Figure 5A). Postabsorptive blood glucose levels were similar through 6 weeks, but diverged by 9 weeks with blood glucose levels lower in Mpc1 LivKO mice (Figure 5B). No significant differences in insulin concentrations were observed (Figure 5C). Analysis of additional post-absorptive and fasting serum parameters following 12 weeks HFD revealed increased post-absorptive ketones and triglycerides and fasting lactate in Mpc1 LivKO mice

(Figure S5A). Differences were not observed in other parameters. Mpc1 LivKO mice manifested superior intraperitoneal glucose tolerance (Figure 5D) without changes in insulin tolerance (Figure 5E), suggesting differences in glucose tolerance were not a result of improved peripheral insulin sensitivity. Together, these results demonstrated that constitutive, liver-specific loss of MPC activity attenuated the development of hyperglycemia and glucose intolerance induced by a high-fat feeding.

Acute *Mpc1* Deletion after Diet-induced Obesity Attenuates Hyperglycemia and Improves Glucose Tolerance

To genetically recapitulate pharmacological liver-specific inhibition and by-pass potential developmental adaptations, we next considered whether acute AAV-mediated hepatic *Mpc1* deletion after entrenched diet-induced obesity would improve glucose homeostasis. Littermate $Mpc1^{fl/fl}$ (WT) mouse pairs were divided into groups to be treated with AAV-Cre or -GFP, expressed from the hepatocyte-specific TBG promoter (Yan et al., 2012). Mice were placed on a high-fat diet for 22 weeks, evaluated for glucose homeostasis, treated with AAV-Cre or -GFP by retro-orbital injection (Figure 5F), and re-evaluated for glucose homeostasis. Prior to AAV administration, no differences were observed between groups that were to receive AAV-Cre or -GFP for glucose tolerance (Figure 5G), insulin tolerance (Figure 5H), and blood glucose excursion (Figure S5B) or lactate clearance (Figure S5C) during a lactate/pyruvate tolerance test.

AAV-Cre but not AAV-GFP resulted in highly-efficient *Mpc1* deletion (Figure S5D). Acute *Mpc1* deletion led to improved glucose (Figure 5I) and insulin (Figure 5J) tolerance. During a lactate/pyruvate tolerance test, blood glucose excursion significantly decreased (Figure S5E) with a strong trend towards decreased lactate clearance (Figure S5F). Furthermore, acute Mpc1 LivKO mice manifested significantly decreased blood glucose values after 4, 6, and 18 hours fasting (Figure 5K). The decrease in blood glucose with 18 hrs fasting was accompanied by a significant decrease in insulin concentrations (Figure 5L). Serum triglycerides were not changed postabsorptively (Figure S5G) but were increased after fasting (Figure S5H). No differences were observed in fasting ketones, lactate, or the AST/ALT ratio (Figure S5H), in hematoxylin- and eosin-stained section lipid droplet area (Figure S5I), fasting liver triglycerides (Figure S5J), or body weight (Figure S5K). These results demonstrated that acute, liver-specific disruption of MPC activity, after longer-term diet-induced obesity attenuated hyperglycemia and improved glucose homeostasis.

Diet-induced Obesity Increases Hepatic MPC expression and Activity

We next investigated whether diet-induced obesity increased MPC activity in the liver. The rationale for this experiment was two-fold. First, pyruvate-driven gluconeogenesis is increased during T2D, which could be partially driven by increased MPC activity. Second, our observations that *Mpc1* deletion in obese but not lean mice decreased blood glucose levels suggested that the MPC may be required for a portion of the increased gluconeogenesis during diet-induced obesity. We isolated liver mitochondria from 22 weeks high fat diet-fed and normal chow-fed, age-matched control mice and measured uptake of ^{14}C-radiolabeled pyruvate and rates of pyruvate and glutamate oxidation. MPC activity was significantly increased with diet-induced obesity (Figure 6A). In contrast, neither

pyruvate nor (Figure 6B) glutamate oxidation (Figure 6C) were increased. Similarly, mitochondrial pyruvate oxidation supported by lower pyruvate concentrations was not increased with 17 weeks high fat feeding (Figure S6A).

We considered whether increased MPC activity resulted from increased MPC expression. Analysis by qPCR revealed *Mpc1* but not *Mpc2* transcript abundance increased with diet-induced obesity (Figure 6D). Interestingly, Western blots of whole liver lysates showed that levels of both Mpc1 and Mpc2 protein increased (Figure S5B), raising the possibility that the increased Mpc1 protein stabilizes and post-transcriptionally increases levels of Mpc2 protein. Western blots of isolated mitochondria showed marked increases in VDAC-normalized Mpc1 and Mpc2 protein, with smaller or no increases in markers of the mitochondrial respiratory chain (Figure 6E). We evaluated whether fasting induced similar increases in MPC activity but none were observed (Figure S5C), suggesting that regulation by fasting may be more complex. Overall, these findings demonstrated that diet-induced obesity resulted in increased MPC activity relative to mitochondrial respiratory capacity, a decoupling which could contribute to increased gluconeogenic drive.

Discussion

Gluconeogenesis is an important process for maintaining blood glucose levels during carbohydrate scarcity and pyruvate is thought to be the major in vivo substrate. Here, we tested the functional importance of the Mitochondrial Pyruvate Carrier encoded by the *Mpc1* and *Mpc2* genes (MPC) for hepatic gluconeogenesis. We demonstrate that the MPC is critical for hepatic mitochondrial pyruvate uptake and gates pyruvate-driven hepatic gluconeogenesis in vivo. These findings link the *Mpc1* and *Mpc2* genes to a fundamental in vivo function at the intersection of cytosolic and mitochondrial metabolism.

Our findings demonstrate the importance of the MPC for efficient regulation of hepatic gluconeogenesis. Pyruvate robustly supports gluconeogenesis and mitochondrial metabolism because it can be converted by single reactions to oxaloacetate or acetyl-CoA, the keystone pair of intermediates required to sustain TCA cycle flux. Glutamine may also be utilized to produce oxaloacetate and acetyl-CoA, but by several reactions and with decreased energetic yield (Yang et al., 2014). Thus, as we observed when MPC activity is lost, regulated increases in gluconeogenesis during fasting that are most efficiently supported by pyruvate may be adaptively supported by less efficient and ammoniagenic glutaminolysis.

Our results illustrate fundamental distinctions between the function of the MPC and the canonical regulators of gluconeogenesis G6pase and PEPCK. First, G6Pase is required for the final step of gluconeogenesis and loss of hepatic G6Pase results in hyper-accumulation of glycogen concomitant with fasting hypoglycemia (Mutel et al., 2011). Second, PEPCK is required for TCA-cycle flux into gluconeogenesis but when disrupted may be circumvented by glycerol-supported gluconeogenesis, at the cost of impaired fatty acid oxidation and severe fasting steatosis (Burgess et al., 2004). Disruption of the MPC imposes neither of these limitations and, as we observed, resulted in neither hepatic glycogen nor lipid accumulation.

Similar distinctions emerge when comparing the MPC to the well-characterized regulators of mitochondrial pyruvate metabolism, pyruvate dehydrogenase (PDH) and pyruvate carboxylase. PDH is required for conversion of pyruvate to acetyl-CoA and essential for glucose oxidation and high rates of amino acid oxidation. Pyruvate carboxylase is required for direct conversion of pyruvate to oxaloacetate for gluconeogenesis and important for sustaining overall TCA cycle flux. In experiments with Mpc1 LivKO mice, we observed decreased but persistent flux of $U^{13}C$-pyruvate into both the M+2 and M+3 isotopomers of TCA-cycle intermediates. Because the M+2 and M+3 isotopomers are markers of PDH activity and the M+3 isotopomer is a marker of pyruvate carboxylase activity, these data indicate that flux through both PDH and pyruvate carboxylase persists when MPC activity is lost. Thus, whereas loss of PDH activity abolishes acetyl-CoA production from non-lipid substrates, substrate transformations to pyruvate within mitochondria enable MPC-independent PDH activity.

Our findings suggest that the liver's high capacity for fatty-acid oxidation and ketogenesis is employed to compensate for loss of MPC activity. The decreased serum cholesterol and fasting triglycerides, increased serum ketones, and decreased dark-period RER we observed in Mpc1 LivKO mice are all consistent with increased hepatic fatty-acid oxidation and decreased lipid synthesis. This is congruent with the increased fatty-acid oxidation induced in cultured myoblasts with MPC knockdown (Vacanti et al., 2014) and likely a general adaptive measure for impaired mitochondrial carbohydrate utilization. Thus, our data support a model for an overall adaptive metabolism where loss of the MPC constrains pathways for mitochondrial pyruvate metabolism and mitochondrially-routed gluconeogenesis to those utilizing amino acids and pyruvate transformations, where fatty-acid oxidation is increased to compensate for decreased mitochondrial pyruvate availability, and where decreased flux of pyruvate through PDH decreases mitochondrial citrate available for efflux into fatty-acid and cholesterol synthesis.

Our data demonstrating that disruption of the MPC improves glucose homeostasis during diet-induced obesity and leads to favorable changes in lipid metabolism recapitulates desired therapeutic outcomes. This raises the question of whether the hepatic MPC may be therapeutically modulated. Indeed, targeting hepatic mitochondria to treat metabolic disease has strong historical and emerging precedent. Metformin, the most widely used and staple treatment for T2D, decreases hepatic gluconeogenesis by perturbing mitochondrial metabolism. Although the precise mechanism remains without consensus, the well-characterized therapeutic effects of metformin provide a convincing demonstration of the potential efficacy of mitochondrial targeting (Madiraju et al., 2014; Miller et al., 2013). As another example, recent findings demonstrate that liver-specific delivery of a mitochondrial uncoupler reversed steatohepatitis and symptoms of diabetes in rats (Perry et al., 2015). More specifically, thiazolidinediones have recently been shown to inhibit MPC activity, presenting the possibility that a portion of their therapeutic effect could result from inhibition of the hepatic MPC (Divakaruni et al., 2013).

Nonetheless, critical considerations must be addressed to determine whether inhibiting the hepatic MPC is a viable therapeutic strategy. The increases in urea cycle activity and blood ketones and slight increases in blood lactate we observed are of unknown clinical

significance, especially when considered in the context of more severe disease or stress conditions like chronic kidney disease, extreme exertion, liver injury or cancer. The decreased mitochondrial pyruvate utilization and increased glutaminolysis with Mpc1 LivKO recapitulates aspects of the transformed metabolism observed in many cancers (Schell et al., 2014; Vacanti et al., 2014; Yang et al., 2014) and could provide a favorable metabolism for tumorigenesis during at risk states like fatty-liver disease or steatohepatitis. Furthermore, disruption of MPC activity in tissues with a lesser capacity for fatty-acid oxidation than the liver, like those of the central nervous system, could be lethal as was observed for a human patient with an inactivating mutation in *MPC1* (Bricker et al., 2012; Brivet et al., 2003).

The increase in hepatic MPC expression and activity we observed with diet-induced obesity may drive increased mitochondrial pyruvate import and therefore elevated gluconeogenesis during T2D. That the MPC is a carrier, rather than a channel, and therefore imposes a kinetic barrier, suggests an evolutionary requirement for limiting the rate of pyruvate entry into mitochondria. This would enable metabolic control beyond that provided directly by regulation of pyruvate carboxylase and pyruvate dehydrogenase. Given that capacity for hepatic pyruvate oxidation in vivo has an upper limit well below that for anaplerotic pyruvate flux, a potential evolutionary basis for controlling uptake is to control anaplerotic flux. From this perspective, an imbalance between mitochondrial pyruvate uptake and oxidation would be expected to proportionally drive gluconeogenesis. This precise phenomenon is observed in T2D and consistent with the increased MPC expression and activity we observe in a mouse model of T2D.

In conclusion, our results demonstrate that the MPC is required for efficient regulation of hepatic gluconeogenesis and whole-body glucose homeostasis. Mpc1 LivKO mice employed adaptive increases in glutaminolysis to sustain fasting euglycemia that elicited increases in urea cycle activity. In mouse models of T2D, compensatory responses to constitutive or acute MPC disruption were insufficient to sustain elevated blood glucose levels. Disruption of the hepatic MPC causes inefficient regulation of gluconeogenesis and broad changes in cellular and systems-level metabolism that decrease hyperglycemia in mouse models of T2D.

Experimental Procedures

Animals and Animal Care

Animal work was performed in accordance with the University of Iowa Animals Use and Care Committee (IACUC). Unless otherwise stated all experiments were performed with 8-12 week old male C57Bl/6 mice. C57Bl/6J mice were purchased from Jackson Laboratories. Sprague-dawley rats were purchased from Harlan Laboratories.

Generation of *Mpc1*$^{fl/fl}$ mice

Mpc1$^{+/fl}$ mouse embryonic stem cells of the C57Bl/6N sub-strain were generated using a knockout-first approach (Skarnes et al., 2011) and obtained from EUCOMM. Recombinant mouse ES cells were injected into blastocysts and implanted into pseudo-pregnant female

mice. Chimeric off-spring were crossed to WT mice of the C57Bl/6J sub-strain to achieve germline transmission of the *Mpc1*^{fl} allele. *Mpc1*$^{+/fl}$ mice used for this study were of a background equivalent to C57Bl/6N mice being back-crossed three times through C57Bl/6J mice.

Tolerance Tests, CLAMS, NMR, and Serum Analysis

Blood glucose and lactate were measured using a One Touch UltraMini glucometer and Nova Biomedical Lactate Plus lactate meter, respectively. Dosages, unless otherwise stated, were based on lean mass, prepared in sterile water, and administered IP. Glucose tolerance test (GTT) – 6hr fast, 2.0g/kg; Lactate/Pyruvate tolerance test (L/PTT) – 18hr fast, 3.0g/kg, 10 lactate:1 pyruvate. Glutamine tolerance test (QTT) - 18hr fast, 2.0 g/kg. Insulin Tolerance Test (ITT) - 4hr fast, 1.5 U/kg Insulin (Humalin, Eli Lilly) in 0.9% saline. Serum parameters were measured using commercially available kits and reagents according to manufacturer's directions.

Traced Hyperinsulinemic Euglycemic Clamps

WT and Mpc1 LivKO mice of age 20 weeks were fasted 18 h and clamped unrestrained and conscious through a jugular vein catheter. Whole-body glucose flux was traced by 0.05μ Ci/min D-[3-^{3}H]-glucose. Insulin was infused at 4 mU/kg/min. Tissue glucose uptake was traced by 10μ Ci [1-^{14}C]-2-deoxy-D-glucose administered 45 minutes before clamp completion.

Mitochondrial Pyruvate Uptake Assay

Mitochondria were isolated similarly to as described previously (Rogers et al., 2011). Mitochondrial pyruvate uptake was measured by the inhibitor stop method (Halestrap, 1975).

Measurements of Mitochondrial Respiration

Experiments measuring mitochondrial respiration were performed using a Seahorse Bioscience XF-96 extracellular flux analyzer similarly to as described previously (Rogers et al., 2011).

Hepatocyte Isolation and Gluconeogenesis Assay

Primary hepatocytes were serum starved overnight (rat) or 3 hours (mouse), incubated in media containing desired substrates and inhibitors or vehicle, and glucose production measured by sampling media at specified times and using the Glucose (HK) Assay Kit (Sigma).

Liver Triglyceride and Glycogen Measurements

Liver triglycerides were extracted similarly to as previously described (Folch et al., 1957) and measured using the Infinity Triglyceride Reagent (Thermo Scientific). Liver glycogen was measured using the acid hydrolysis approach (Passonneau and Lauderdale, 1974) and with the Glucose (HK) Assay Kit (Sigma).

Stable-isotope Tracer Metabolomics

Glucose concentrations and ^{13}C-Mass isotopomer enrichment was determined as previously described (Sunny and Bequette, 2010). Organic and amino acids were determined as previously described (Des Rosiers et al., 1994; Molnár-Perl and Katona, 2000; Sobolevsky et al., 2003).

Steady-State Metabolomics

Steady metabolic analysis was performed as previously reported (A et al., 2005; Cox et al., 2009).

qPCR

RNA was extracted using TRIzol (Life Technologies). RNA was reverse transcribed using *H*igh-Capacity cDNA Reverse Transcription Kit (Applied Biosystems) followed by qPCR reactions using SYBR Green (Life Technologies).

Data Analysis

Unless otherwise noted, all data are reported as Mean ± SEM. SigmaPlot and Microsoft Excel software was used to perform statistical analysis, which was by t-test unless otherwise stated. Significance was defined as indicated.

Supplementary Material

Refer to Web version on PubMed Central for supplementary material.

Acknowledgements

We thank Brett Wagner for assistance running the Seahorse Bioscience XF96, Jamie Soto and Jianrong Yao of the Fraternal Order of the Eagles Diabetes Research Center (FOEDRC) Metabolic Phenotypic Core for assistance with insulin clamps, and Charles Brenner and Brandon Davies of the Department of Biochemistry for carefully reading a draft manuscript and providing helpful feedback. This work was supported by NIH grants R01 DK104998 (EBT), R00 AR059190 (EBT), R01 DK078184 (SCB), R24 DK096518 (AWN), R01 GM094232 (JR), F32 DK101183 (LRG), T32 HL007121 to Francois Abboud (LRG), T32 HL007638 to Michael Welsh (AJR), P30CA086862 to George Weiner, which contributed to support of core facilities utilized for this research, the Carver College of Medicine NIH-funded MSTP Training Program GM007337 (SCT), the Robert A. Welch Foundation (SCB), A FOEDRC Faculty Research Scholar (AWN), an Edward Mallinckrodt Jr. Foundation Grant (MJP), an American Diabetes Association Junior Faculty Award (MJP), and a Carver College of Medicine Collaborative Pilot Grant (EBT and MJP).

References

A J, Trygg J, Gullberg J, Johansson AI, Jonsson P, Antti H, Marklund SL, Moritz T. Extraction and GC/MS analysis of the human blood plasma metabolome. Anal Chem. 2005; 77:8086–8094. [PubMed: 16351159]

Bender T, Pena G, Martinou JC. Regulation of mitochondrial pyruvate uptake by alternative pyruvate carrier complexes. EMBO J. 2015

Beuster G, Zarse K, Kaleta C, Thierbach R, Kiehntopf M, Steinberg P, Schuster S, Ristow M. Inhibition of alanine aminotransferase in silico and in vivo promotes mitochondrial metabolism to impair malignant growth. J Biol Chem. 2011; 286:22323–22330. [PubMed: 21540181]

Bricker DK, Taylor EB, Schell JC, Orsak T, Boutron A, Chen YC, Cox JE, Cardon CM, Van Vranken JG, Dephoure N, et al. A mitochondrial pyruvate carrier required for pyruvate uptake in yeast, Drosophila, and humans. Science. 2012; 337:96–100. [PubMed: 22628558]

Brivet M, Garcia-Cazorla A, Lyonnet S, Dumez Y, Nassogne MC, Slama A, Boutron A, Touati G, Legrand A, Saudubray JM. Impaired mitochondrial pyruvate importation in a patient and a fetus at risk. Mol Genet Metab. 2003; 78:186–192. [PubMed: 12649063]

Burgess SC, Hausler N, Merritt M, Jeffrey FM, Storey C, Milde A, Koshy S, Lindner J, Magnuson MA, Malloy CR, et al. Impaired tricarboxylic acid cycle activity in mouse livers lacking cytosolic phosphoenolpyruvate carboxykinase. J Biol Chem. 2004; 279:48941–48949. [PubMed: 15347677]

Burgess SC, He T, Yan Z, Lindner J, Sherry AD, Malloy CR, Browning JD, Magnuson MA. Cytosolic phosphoenolpyruvate carboxykinase does not solely control the rate of hepatic gluconeogenesis in the intact mouse liver. Cell Metab. 2007; 5:313–320. [PubMed: 17403375]

Cox J, Williams S, Grove K, Lane RH, Aagaard-Tillery KM. A maternal high-fat diet is accompanied by alterations in the fetal primate metabolome. Am J Obstet Gynecol. 2009; 201:281, e281–289. [PubMed: 19733280]

Des Rosiers C, Fernandez CA, David F, Brunengraber H. Reversibility of the mitochondrial isocitrate dehydrogenase reaction in the perfused rat liver. Evidence from isotopomer analysis of citric acid cycle intermediates. J Biol Chem. 1994; 269:27179–27182. [PubMed: 7961626]

Divakaruni AS, Wiley SE, Rogers GW, Andreyev AY, Petrosyan S, Loviscach M, Wall EA, Yadava N, Heuck AP, Ferrick DA, et al. Thiazolidinediones are acute, specific inhibitors of the mitochondrial pyruvate carrier. Proc Natl Acad Sci U S A. 2013; 110:5422–5427. [PubMed: 23513224]

Folch J, Lees M, Sloane Stanley GH. A simple method for the isolation and purification of total lipids from animal tissues. J Biol Chem. 1957; 226:497–509. [PubMed: 13428781]

Forest CD, O'Brien RM, Lucas PC, Magnuson MA, Granner DK. Regulation of phosphoenolpyruvate carboxykinase gene expression by insulin. Use of the stable transfection approach to locate an insulin responsive sequence. Mol Endocrinol. 1990; 4:1302–1310. [PubMed: 2172798]

Halestrap AP. The mitochondrial pyruvate carrier. Kinetics and specificity for substrates and inhibitors. Biochem J. 1975; 148:85–96. [PubMed: 1156402]

Halestrap AP, Denton RM. The specificity and metabolic implications of the inhibition of pyruvate transport in isolated mitochondria and intact tissue preparations by alpha-Cyano-4-hydroxycinnamate and related compounds. Biochem J. 1975; 148:97–106. [PubMed: 1171687]

Herzig S, Raemy E, Montessuit S, Veuthey JL, Zamboni N, Westermann B, Kunji ER, Martinou JC. Identification and functional expression of the mitochondrial pyruvate carrier. Science. 2012; 337:93–96. [PubMed: 22628554]

Katz J, Tayek JA. Recycling of glucose and determination of the Cori Cycle and gluconeogenesis. Am J Physiol. 1999; 277:E401–407. [PubMed: 10484349]

Kumashiro N, Beddow SA, Vatner DF, Majumdar SK, Cantley JL, Guebre-Egziabher F, Fat I, Guigni B, Jurczak MJ, Birkenfeld AL, et al. Targeting pyruvate carboxylase reduces gluconeogenesis and adiposity and improves insulin resistance. Diabetes. 2013; 62:2183–2194. [PubMed: 23423574]

Madiraju AK, Erion DM, Rahimi Y, Zhang XM, Braddock DT, Albright RA, Prigaro BJ, Wood JL, Bhanot S, MacDonald MJ, et al. Metformin suppresses gluconeogenesis by inhibiting mitochondrial glycerophosphate dehydrogenase. Nature. 2014; 510:542–546. [PubMed: 24847880]

Mendes-Mourão J, Halestrap A, Crisp DM, Pogson CI. The involvement of mitochondrial pyruvate transport in the pathways of gluconeogenesis from serine and alanine in isolated rat and mouse liver cells. FEBS Letters. 1975; 53:29–32. [PubMed: 1140393]

Merritt ME, Harrison C, Sherry AD, Malloy CR, Burgess SC. Flux through hepatic pyruvate carboxylase and phosphoenolpyruvate carboxykinase detected by hyperpolarized 13C magnetic resonance. Proc Natl Acad Sci U S A. 2011; 108:19084–19089. [PubMed: 22065779]

Miller RA, Chu Q, Xie J, Foretz M, Viollet B, Birnbaum MJ. Biguanides suppress hepatic glucagon signalling by decreasing production of cyclic AMP. Nature. 2013; 494:256–260. [PubMed: 23292513]

Molnár-Perl I, Katona ZF. GC-MS of amino acids as their trimethylsilyl/tbutyldimethylsilyl Derivatives: In model solutions III. Chromatographia. 2000; 51:S228–S236.

Mutel E, Abdul-Wahed A, Ramamonjisoa N, Stefanutti A, Houberdon I, Cavassila S, Pilleul F, Beuf O, Gautier-Stein A, Penhoat A, et al. Targeted deletion of liver glucose-6 phosphatase mimics

glycogen storage disease type 1a including development of multiple adenomas. J Hepatol. 2011; 54:529–537. [PubMed: 21109326]

Pande SV, Parvin R. Pyruvate and acetoacetate transport in mitochondria. A reappraisal. J Biol Chem. 1978; 253:1565–1573. [PubMed: 627555]

Passonneau JV, Lauderdale VR. A comparison of three methods of glycogen measurement in tissues. Anal Biochem. 1974; 60:405–412. [PubMed: 4844560]

Perry RJ, Zhang D, Zhang XM, Boyer JL, Shulman GI. Controlled-release mitochondrial protonophore reverses diabetes and steatohepatitis in rats. Science. 2015; 347:1253–1256. [PubMed: 25721504]

Postic C, Shiota M, Niswender KD, Jetton TL, Chen Y, Moates JM, Shelton KD, Lindner J, Cherrington AD, Magnuson MA. Dual roles for glucokinase in glucose homeostasis as determined by liver and pancreatic beta cell-specific gene knock-outs using Cre recombinase. J Biol Chem. 1999; 274:305–315. [PubMed: 9867845]

Potthoff MJ, Boney-Montoya J, Choi M, He T, Sunny NE, Satapati S, Suino-Powell K, Xu HE, Gerard RD, Finck BN, et al. FGF15/19 regulates hepatic glucose metabolism by inhibiting the CREB-PGC-1alpha pathway. Cell Metab. 2011; 13:729–738. [PubMed: 21641554]

Rogers GW, Brand MD, Petrosyan S, Ashok D, Elorza AA, Ferrick DA, Murphy AN. High throughput microplate respiratory measurements using minimal quantities of isolated mitochondria. PLoS One. 2011; 6:e21746. [PubMed: 21799747]

Schell JC, Olson KA, Jiang L, Hawkins AJ, Van Vranken JG, Xie J, Egnatchik RA, Earl EG, DeBerardinis RJ, Rutter J. A role for the mitochondrial pyruvate carrier as a repressor of the Warburg effect and colon cancer cell growth. Mol Cell. 2014; 56:400–413. [PubMed: 25458841]

Skarnes WC, Rosen B, West AP, Koutsourakis M, Bushell W, Iyer V, Mujica AO, Thomas M, Harrow J, Cox T, et al. A conditional knockout resource for the genome-wide study of mouse gene function. Nature. 2011; 474:337–342. [PubMed: 21677750]

Sobolevsky TG, Revelsky AI, Miller B, Oriedo V, Chernetsova ES, Revelsky IA. Comparison of silylation and esterification/acylation procedures in GC-MS analysis of amino acids. Journal of Separation Science. 2003; 26:1474–1478.

Sunny NE, Bequette BJ. Gluconeogenesis differs in developing chick embryos derived from small compared with typical size broiler breeder eggs. J Anim Sci. 2010; 88:912–921. [PubMed: 19966165]

Terrettaz J, Jeanrenaud B. Contribution of glycerol and alanine to basal hepatic glucose production in the genetically obese (fa/fa) rat. Biochem J. 1990; 270:803–807. [PubMed: 2241912]

Thomas AP, Halestrap AP. The role of mitochondrial pyruvate transport in the stimulation by glucagon and phenylephrine of gluconeogenesis from L-lactate in isolated rat hepatocytes. Biochem J. 1981; 198:551–560. [PubMed: 7326022]

Vacanti NM, Divakaruni AS, Green CR, Parker SJ, Henry RR, Ciaraldi TP, Murphy AN, Metallo CM. Regulation of substrate utilization by the mitochondrial pyruvate carrier. Mol Cell. 2014; 56:425–435. [PubMed: 25458843]

Vigueira PA, McCommis KS, Schweitzer GG, Remedi MS, Chambers KT, Fu X, McDonald WG, Cole SL, Colca JR, Kletzien RF, et al. Mitochondrial pyruvate carrier 2 hypomorphism in mice leads to defects in glucose-stimulated insulin secretion. Cell Rep. 2014; 7:2042–2053. [PubMed: 24910426]

Xia J, Mandal R, Sinelnikov IV, Broadhurst D, Wishart DS. MetaboAnalyst 2.0--a comprehensive server for metabolomic data analysis. Nucleic Acids Res. 2012; 40:W127–133. [PubMed: 22553367]

Yan Z, Yan H, Ou H. Human thyroxine binding globulin (TBG) promoter directs efficient and sustaining transgene expression in liver-specific pattern. Gene. 2012; 506:289–294. [PubMed: 22820390]

Yang C, Ko B, Hensley CT, Jiang L, Wasti AT, Kim J, Sudderth J, Calvaruso MA, Lumata L, Mitsche M, et al. Glutamine oxidation maintains the TCA cycle and cell survival during impaired mitochondrial pyruvate transport. Mol Cell. 2014; 56:414–424. [PubMed: 25458842]

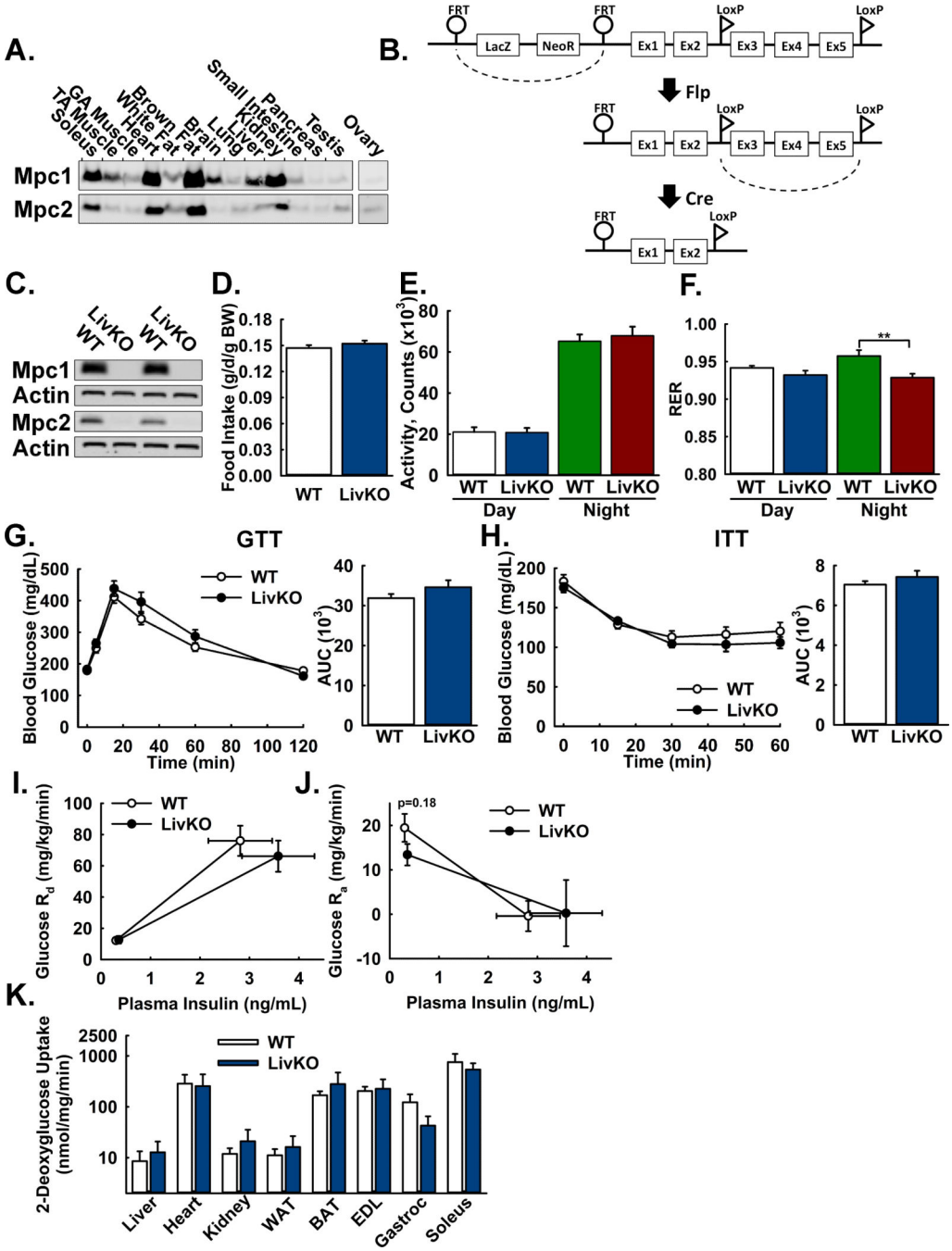

Figure 1. Generation and basic characterization of mice with liver-specific deletion of *Mpc1*

A: Western Blot analysis of Mpc1 and Mpc2 protein abundance in lysates of C57Bl/6J mouse tissues. Loading was normalized to total protein. A reference protein is not shown because of nonuniform expression among different tissues.

B: Scheme illustrating generation of the *Mpc1* null allele.

C: Western blot analysis of Mpc1 and Mpc2 protein abundance in liver lysates from WT and Mpc1 LivKO mice. Loading was normalized to total protein and actin is utilized as a reference protein.

D: Daily food intake by WT and Mpc1 LivKO mice, normalized to body weight (BW). (n=8)
E: Voluntary physical activity, measured by beam breaks in CLAMS cages, of WT and Mpc1 LivKO mice. (n=8)
F: Respiratory Exchange Ratio (RER) of WT and Mpc1 LivKO mice. (n=8)
G,H: Glucose (G) and insulin (H) tolerance tests comparing WT and Mpc1 LivKO mice. Blood glucose was measured serially and an AUC calculated. (n=8)
I: Glucose disposal rate (Rd) versus serum insulin during the basal and hyperinsulinemic sampling portions of the clamp. (n=5-6)
J: Glucose appearance rate (Ra) versus serum insulin during the basal and hyperinsulinemic sampling portions of the clamp. (n=5-6)
K: Insulin-stimulated uptake of 2-deoxyglucose during the terminal hyperinsulinemic portion of the clamp. (n=5-6)
Data are presented as mean ± SEM (*$p<0.05$, **$p<0.01$). Also see Figure S1.

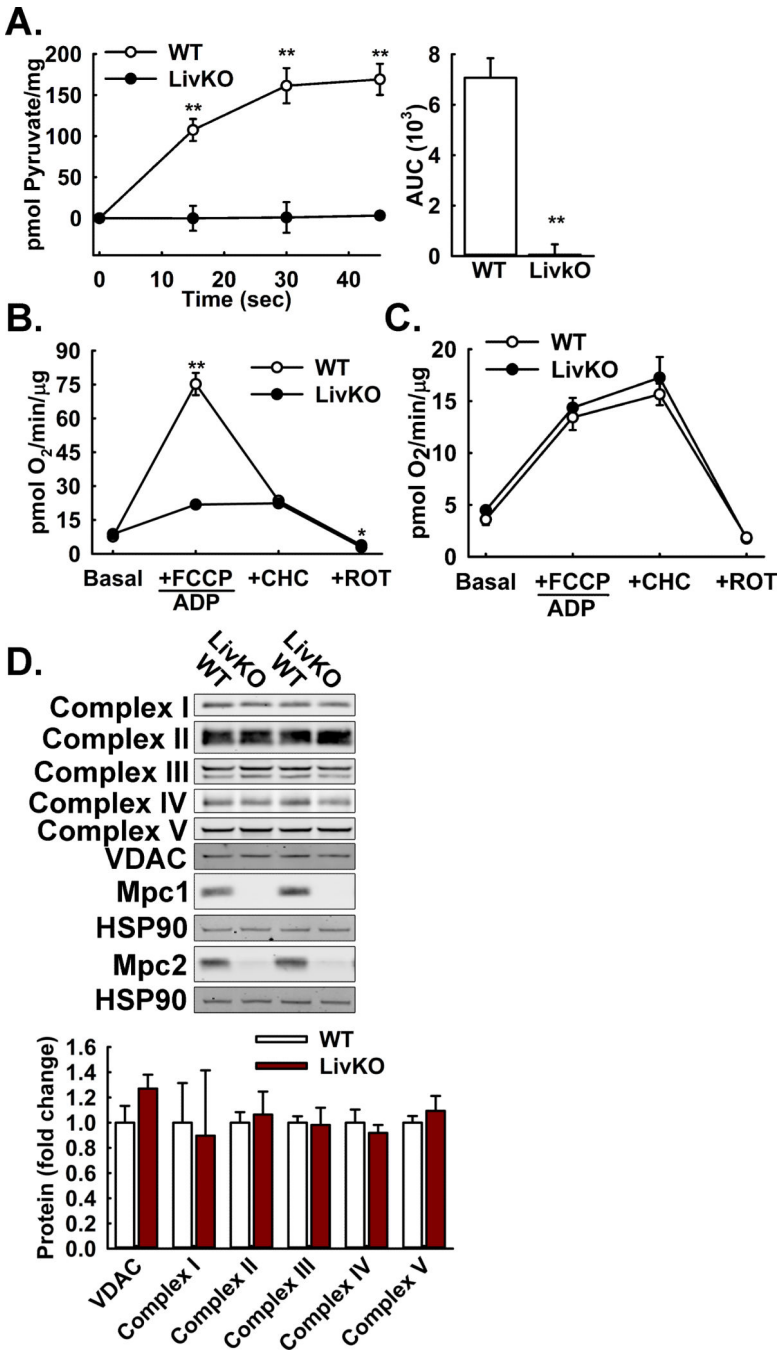

Figure 2. Effects of *Mpc1* deletion on hepatic mitochondrial pyruvate metabolism

A: ^{14}C-Pyruvate uptake by liver mitochondria isolated from WT and Mpc1 LivKO mice. (n=4)

B: Pyruvate-driven (10 mM pyruvate/2 mM malate) respiration by liver mitochondria isolated from WT and Mpc1 LivKO mice. (n=4)

C: Glutamate-driven (10 mM glutamate/2 mM malate) respiration by liver mitochondria isolated from WT and Mpc1 LivKO mice. (n=4)

D: Western blot analysis of electron transport chain (ETC) components (Complex I-V), and Mpc1, Mpc2, VDAC, and HSP90 proteins in liver lysates from WT and Mpc1 LivKO mice. Densitometric quantification is relative to HSP90.

Data are presented as mean ± SEM (**p<0.01). Also see Figure S2.

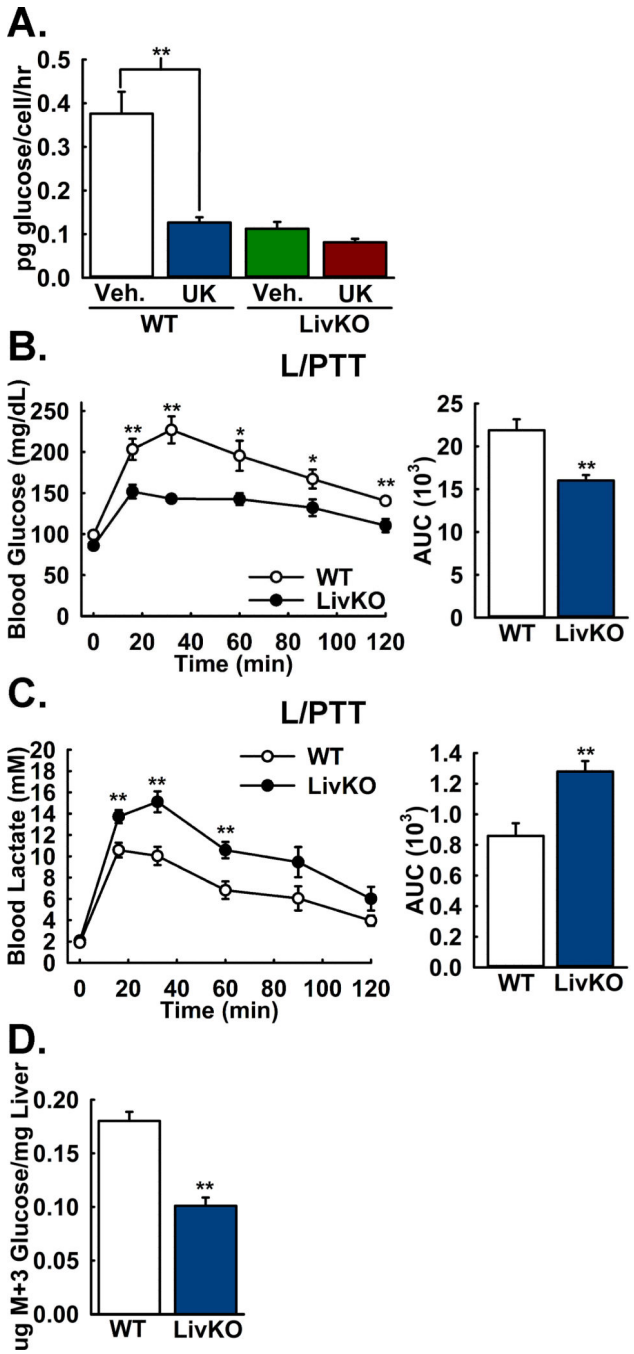

Figure 3. Lactate/pyruvate-driven gluconeogenesis is MPC-dependent

A: Lactate/pyruvate-driven gluconeogenesis by mouse primary hepatocytes isolated from WT and LivKO mice, in the presence of the MPC-inhibitor UK5099 (UK) or vehicle (Veh). (n=3)

B,C: Blood (B) glucose excursion and (C) lactate clearance in WT and Mpc1 LivKO mice during a lactate/pyruvate tolerance test (L/PTT). Blood glucose and lactate were measured serially and AUCs calculated. (n=8)

D: M+3 glucose concentrations in liver tissue from WT and Mpc1 LivKO mice following administration of $U^{13}C$-labeled lactate/pyruvate. (n=6)
Data are presented as mean ± SEM (*p<0.05, **p<0.01).

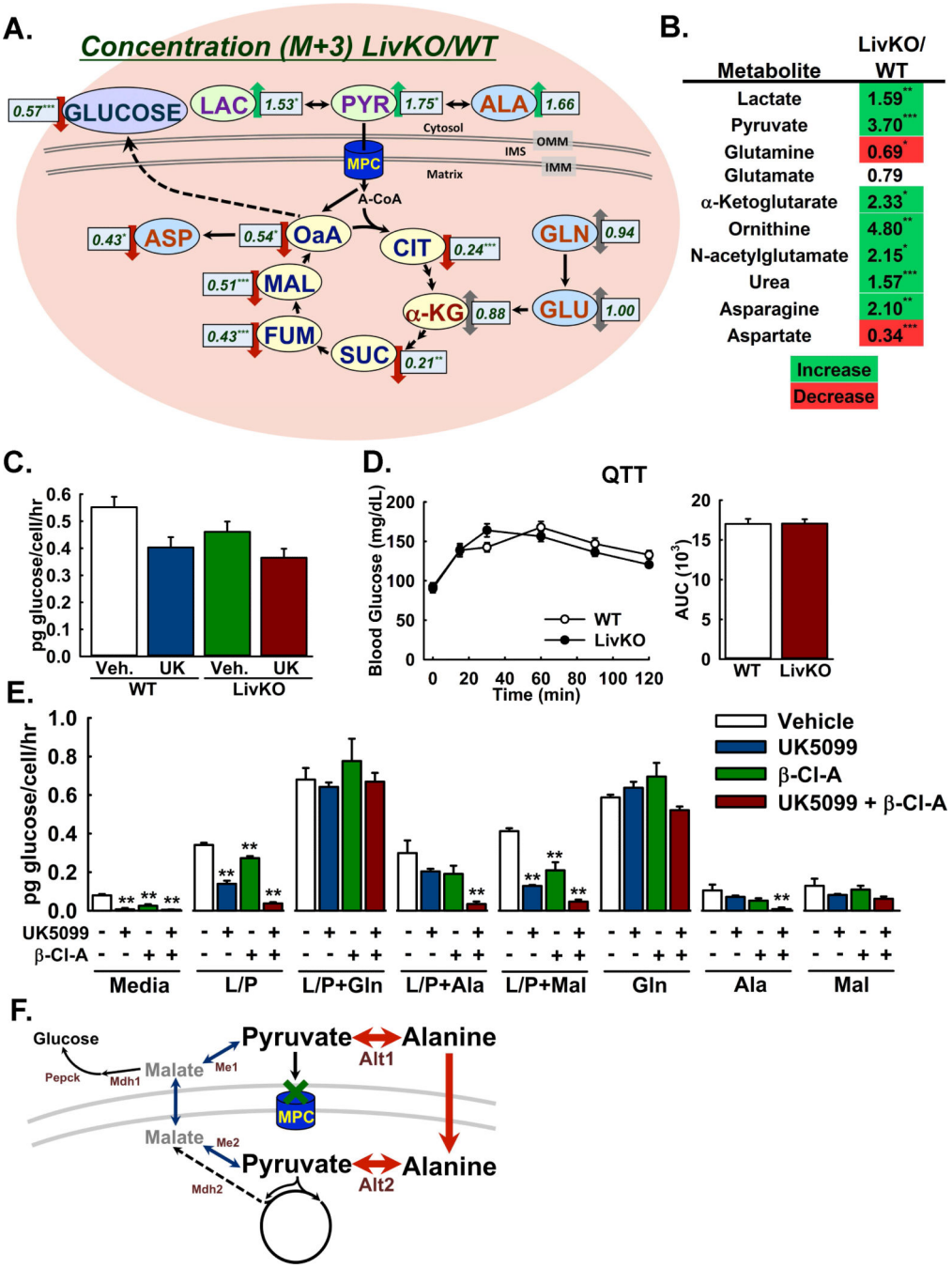

Figure 4. Glutaminolysis and pyruvate transformations enable MPC-independent gluconeogenesis

A: Ratios of absolute M+3 isotopomer concentrations in Mpc1 LivKO versus WT livers (LivKO/WT) following administration of U^{13}C-labeled lactate/pyruvate. (n=5-6)

B: Relative steady-state abundance of select metabolites in Mpc1 LivKO versus WT livers (LivKO/WT) after 18h fasting. (n=7-9)

C: Glutamine-driven gluconeogenesis by mouse primary hepatocytes isolated from WT and Mpc1 LivKO mice, in the presence of the MPC-inhibitor UK5099 (UK) or vehicle (Veh). (n=3)

D: Glutamine tolerance test (QTT) comparing WT and Mpc1 LivKO mice. Blood glucose was measured serially and an AUC calculated. (n=9)
E: Gluconeogenesis by rat primary hepatocytes, supported by different substrates and treated with vehicle, the MPC inhibitor UK5099, the ALT-inhibitor β-Cl-A, or both. L/P: 4.5mM lactate/0.5mM pyruvate; L/P+Gln: 2.25mM lactate/0.25mM pyruvate + 2.5mM glutamine; L/P+Ala: 2.25mM lactate/0.25mM pyruvate + 2.5mM alanine; Gln: 5mM glutamine; Ala: 5mM alanine; and Mal: 5mM malate. (n=3)
F: Model for pyruvate transformations to alanine and malate as MPC by-passes. Me1/2, malic enzyme (cytosolic/mitochondrial); Alt1/2, alanine transaminase (cytosolic/mitochondrial); Mdh1/2, malate dehydrogenase (cytosolic/mitochondrial); Pepck, phosphoenolpyruvate carboxykinase 1. Data are presented as mean ± SEM ($p<0.05$, $^{**}p<0.01$, $^{***}p<0.001$). Also see Figure S3, Table S1, and Table S2.

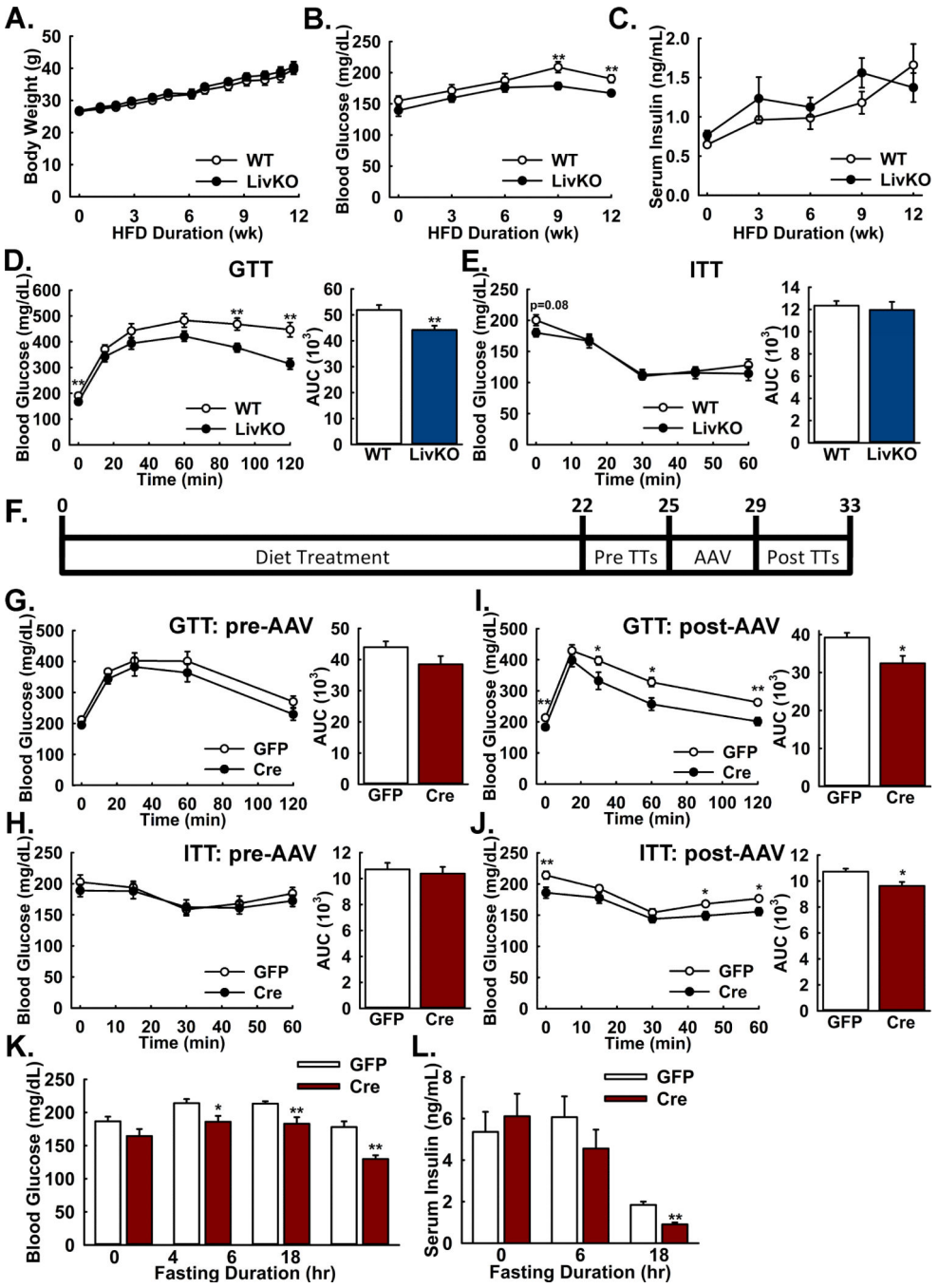

Figure 5. Both constitutive and acute *Mpc1* deletion attenuate hyperglycemia and glucose intolerance during high-fat diet induced obesity

A: Body weights of WT and Mpc1 LivKO mice over 12 weeks of high fat diet (HFD) feeding. (n=10)

B,C: Postabsorptive blood (B) glucose and (C) insulin levels of WT and Mpc1 LivKO mice over 12 weeks of HFD. (n=10)

D,E: Glucose (D) and insulin (E) tolerance tests comparing WT and Mpc1 LivKO mice after 12 weeks of HFD. Blood glucose was measured serially and an AUC calculated. (n=10)

F: Schema illustrating the time-course of high fat feeding, tolerance test (TT) administration, and AAV-GFP/Cre administration for *Mpc1*$^{fl/fl}$ mice.

G,H: Glucose (G) and insulin (H) tolerance tests comparing groups of HFD *Mpc1*$^{fl/fl}$ before treatment with either AAV-GFP or AAV-Cre. Blood glucose was measured serially and an AUC calculated. (n = 10)

I,J: Glucose (I) and insulin (J) tolerance tests comparing groups of HFD *Mpc1*$^{fl/fl}$ mice after treatment with either AAV-GFP or AAV-Cre and hepatocyte-specific *Mpc1* deletion in AAV-Cre treated mice. Blood glucose was measured serially and an AUC calculated. (n = 10)

K: Blood glucose levels in AAV-GFP- and AAV-Cre-treated mice after 0, 4, 6, and 18 hours of fasting. (n=10)

L: Serum insulin levels in AAV-GFP- and AAV-Cre-treated mice after 0, 6, and 18 of fasting. (n=5-10)

Data are presented as mean ± SEM (*p<0.05, **p<0.01). Also see Figure S5.

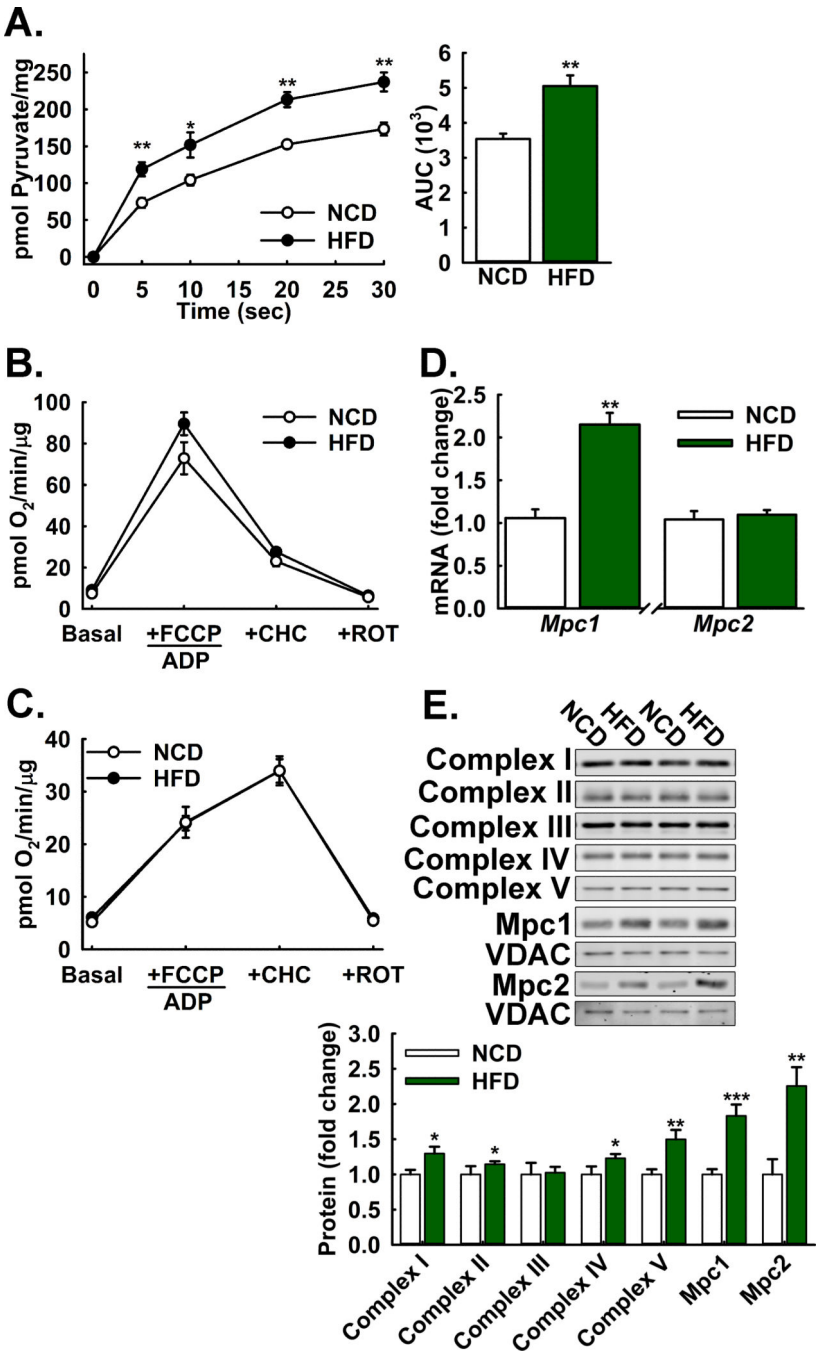

Figure 6. Diet-induced obesity increases hepatic MPC protein levels and Activity

A: ^{14}C-Pyruvate uptake by liver mitochondria isolated from high fat-diet fed versus age-matched normal chow fed control mice. (n=8)

B,C: (B) Pyruvate-driven (10 mM pyruvate/2 mM malate) and (C) glutamate-driven (10 mM glutamate/2 mM malate) respiration by liver mitochondria isolated from high fat-diet fed versus age-matched normal chow-fed control mice (n=8).

D: Relative *Mpc1* and *Mpc2* transcript abundance in livers of high fat-diet fed versus age-matched normal chow-fed control mice, normalized to *U36b4*. (n=8)

E: Western blot analysis of electron transport chain (ETC) components (Complex I-V), and Mpc1, Mpc2, VDAC, and HSP90 proteins in liver lysates from high fat-diet fed versus age-matched normal chow-fed control mice. Densitometric quantification is relative to HSP90. (n=8)

All mice were on a high-fat diet for 22 weeks from 6 weeks of age. Data are presented as mean ± SEM (*p<0.05, **p<0.01, ***p<0.001). Also see Figure S6.

		4 hr Fast		18hr Fast		
		WT	**LivKO**	**WT**	**LivKO**	
Serum	Insulin	0.68 ± 0.03	0.69 ± 0.03	0.18 ± 0.01	0.16 ± 0.02	ng/mL
	Triglycerides	50.0 ± 1.2	57.7 ± 1.8**	75.0 ± 6.2	51.3 ± 2.0**	mg/dL
	NEFAs	0.84 ± 0.04	0.92 ± 0.06	1.09 ± 0.07	0.89 ± 0.03	mEq/L
	Cholesterol	145.3 ± 4.9	122.6 ± 4.3**	142.4 ± 4.1	119.0 ± 3.8**	mg/dL
	Ketones	191.0 ± 22.0	355.2 ± 16.9**	708.1 ± 42.6	1006.6 ± 31.8*	µmol/L
	Lactate	2.24 ± 0.16	2.75 ± 0.16*	1.19 ± 0.05	1.94 ± 0.14**	mmol/L
	Glucose	148.6 ± 5.3	132.4 ± 4.1*	94.1 ± 4.2	88.8 ± 5.6	mg/dL
	AST/ALT	1.75 ± 0.14	1.77 ± 0.14	1.84 ± 0.12	1.85 ± 0.12	
Liver	Triglycerides	10.0 ± 1.27	11.5 ± 0.9	48.1 ± 2.6	51.2 ± 1.9	mg/g
	Glycogen (glucose)	87.3 ± 15.3	65.7 ± 16.7	30.7 ± 4.8	31.7 ± 4.0	µmol/g

Data are mean ± SEM

* = p<0.05

** = p<0.01